Atmos. Chem. Phys. Discuss., 11, 31643–31688, 2011
www.atmos-chem-phys-discuss.net/11/31643/2011/
doi:10.5194/acpd-11-31643-2011

Atmospheric Chemistry and Physics Discussions

The equilibrium response to idealized thermal forcings in a comprehensive GCM: implications for recent tropical expansion

R. J. Allen[1,2,3], **S. C. Sherwood**[4], **J. R. Norris**[2], **and C. S. Zender**[3]

[1]Department of Earth Sciences, University of California, Riverside, Riverside, CA, USA
[2]Scripps Institution of Oceanography, University of California, San Diego, CA, USA
[3]Department of Earth System Science, University of California, Irvine, CA, USA
[4]Climate Change Research Centre, University of New South Wales, Sydney, Australia

Received: 17 August 2011 – Accepted: 19 November 2011 – Published: 2 December 2011

Correspondence to: R. J. Allen (rjallen@ucr.edu)

Published by Copernicus Publications on behalf of the European Geosciences Union.

Abstract

Several recent studies have shown the width of the tropical belt has increased over the last several decades. The mechanisms driving tropical expansion are not well known and the recent expansion is underpredicted by state-of-the art GCMs. We use the CAM3 GCM to investigate how tropical width responds to idealized atmospheric heat sources, focusing on zonal displacement of the tropospheric jets (TJ). The heat sources include global and zonally restricted lower-tropospheric warmings and stratospheric coolings, which coarsely represent possible impacts of ozone or aerosol changes. Similar to prior studies with simplified GCMs, we find that stratospheric cooling-particularly at high-latitudes-shifts jets poleward and excites Northern and Southern Annular Mode (NAM/SAM)-type responses. We also find, however, that modest heating of the mid-latitude boundary layer drives a similar response; heating at high latitudes provokes a weaker, equatorward shift and tropical heating produces no shift. Responses to stratospheric cooling are consistent with a wave-mean flow interaction involving increased wave refraction, and downward propagation of the stratospheric wind anomaly. Over 70 % of the variance in annual mean jet displacements across 27 experiments, however, is accounted for by a newly proposed "Expansion Index", which compares mid-latitude tropospheric warming to that at other latitudes. We find that previously proposed factors, including tropopause height and tropospheric stability, do not fully explain the results. Results suggest recently observed tropical expansion could have been driven not only by stratospheric cooling, but also by mid-latitude heating sources due for example to ozone or aerosol changes.

1 Introduction

Recent observational analyses show the tropics have widened over the last several decades. Estimates range from 2–5° latitude since 1979 (Seidel et al., 2008) and are based on several metrics, including a poleward shift of the Hadley cell (Hu and

ACPD
11, 31643–31688, 2011

Fu, 2007), increased frequency of high tropopause days in the subtropics (Seidel and Randel, 2007) and increased width of the region with tropical column ozone levels (Hudson et al., 2006). Studies have also inferred a poleward shift in the tropospheric jets (TJ), based on enhanced warming in the mid-latitude troposphere (Fu et al., 2006) and cooling in the mid-latitude stratosphere (Fu and Lin, 2011). Zhou et al. (2011) showed a poleward shift of cloud boundaries associated with the Hadley cell, as well as a poleward shift of the subtropical dry zones. Clearly, tropical expansion has important implications for both global, and regional climate.

Climate models also show current, and future, global warming is associated with tropical expansion. Using the Intergovernmental Panel on Climate Change (IPCC) Coupled Model Intercomparison Project, Phase 3 (CMIP3) simulations, Yin (2005) found a poleward shift in the mid-latitude storm tracks, which was accompanied by poleward shifts in surface wind stress and precipitation. Similarly, Lorenz and DeWeaver (2007) found a poleward shift (and strengthening) of the tropospheric jets in response to global warming, which was accompanied by poleward and upward shifts in transient kinetic energy and momentum flux. Lu et al. (2007) showed CMIP3 models yield poleward displacement (and weakening) of the Hadley cell and subtropical dry zones, which is associated with an increase in extratropical tropopause height, and subtropical static stability. Models also show that tropical expansion projects onto the leading pattern of variability (Kushner et al., 2001), with about half of CMIP3 model-simulated Hadley cell and subtropical dry zone expansion during the next century explained by positive trends in the Northern and Southern Annular Mode (NAM/SAM) (Previdi and Liepert, 2007).

Although both GCMs and observations show tropical widening over the last 2–3 decades, models underestimate the magnitude of observed trends. For example, Johanson and Fu (2009) show the largest CMIP3 tropical widening trends are ~1/5 of the observed widening. This significant underestimation exists across five scenarios, as well as three separate definitions of Hadley cell width, including dynamical and hydrological definitions. Lu et al. (2009) used the GFDL atmospheric model AM2.1

ACPD
11, 31643–31688, 2011

to show observed changes in sea surface temperatures (SSTs) and sea-ice cannot explain increased tropical width, as defined by the tropopause probability density function. A similar simulation, however, that also included the direct radiative effects of anthropogenic and natural sources better reproduced the observed widening. Polvani et al. (2011) showed that broadening of the Hadley cell and poleward expansion of the subtropical dry zone over the latter half of the 20th century in the SH – particularly during December-January-February – have been primarily caused by polar stratospheric ozone depletion.

Idealized climate models (e.g. no moist processes, no topography) have been used to better understand the mechanisms involved with tropical expansion. Polvani and Kushner (2002) and Kushner and Polvani (2004) found that cooling of the polar winter stratosphere, which is associated with reduced stratospheric wave drag, results in a poleward tropospheric jet shift and strengthening of surface wind. Haigh et al. (2005) showed that uniform heating of the stratosphere (e.g. via increased solar or volcanic activity), or heating restricted to high-latitudes, forces the jets equatorward; heating in low latitudes forces them poleward.

Frierson et al. (2007) used both simple and comprehensive GCMs to show tropical expansion occurs with increased global mean temperature, and secondly, with an increased pole-to-equator temperature gradient. They argued that the response was due to increased static stability, which reduces baroclinic growth rates and pushes the latitude of baroclinic instability onset poleward, in agreement with the Hadley cell width scaling of Held (2000). This was further supported by Lu et al. (2008), who showed that poleward expansion of the Hadley cell and shift of the eddy-driven jet in CMIP3 global warming experiments are related to a reduction in baroclinicity, which is primarily caused by an increase in subtropical static stability. This relationship was most significant during austral summer (December-January-February), particularly in the Southern Hemisphere (SH).

Lorenz and DeWeaver (2007) showed that increasing the tropopause height (as expected in a warmer troposphere) in a simple dry GCM resulted in poleward jet

ACPD
11, 31643–31688, 2011

displacement. This response was largest when the tropopause on the poleward flank of the jet was raised; however, the opposite response occurred if the tropopause was raised on the equatorward side of the jet. This tropopause-jet relationship is consistent with Williams (2006).

Recently, Butler et al. (2010) used a simplified GCM to try to attribute storm track shifts to warming in particular regions. They found that warming in the tropical troposphere, or cooling in the high-latitude stratosphere, each shifted the storm tracks poleward, whereas polar warming shifted them equatorward. A similar response to tropical tropospheric warming was found by Butler et al. (2011) and Wang et al. (2011). Such results are qualitatively consistent with earlier studies (Chen and Held, 2007; Chen et al., 2008), arguing that the observed poleward shift in the surface westerlies has been due to increased Rossby wave phase speeds, which results in poleward displacement of the region of wave breaking in the subtropics. Kidston et al. (2011) argued that an increase in eddy length scale, a robust response to global warming (Kidston et al., 2010), causes the poleward shift of the mid-latitude eddy-driven jet streams.

Expanding upon these studies, we use a comprehensive GCM to gain a better understanding of how tropical width – particularly tropospheric (850–300 hPa) jet displacement – responds to different types of simple heating at realistic amplitudes. The thermal forcings examined include zonally uniform heat sources in the troposphere or heat sinks in the stratosphere. Our study differs from past studies in specifying heat sources that are representative of possible non-CO_2 climatic forcings, rather than imposing characteristic temperature perturbations. Investigation of the effects of such heat sources on tropical width is of interest due to the significant 20th century increases in anthropogenic aerosols, including absorbing aerosols like black carbon (Bond et al., 2007) and reflecting aerosols like sulfate (Smith et al., 2011), as well as tropospheric ozone (Shindell et al., 2006) and ozone precursors (van Aardenne et al., 2001). Our objective is to clarify the sensitivity of tropical width to different types of heating, with the ultimate goals of gaining insight into the observed widening and better understanding

ACPD
11, 31643–31688, 2011

of the responses seen in past GCM studies. Our results show the importance of meridional temperature gradients and wave-mean flow interaction in driving zonal jet displacements. We also show that previously proposed tropical expansion mechanisms are unable to fully explain our results. We build upon these results in a subsequent paper, which will examine the responses to more realistic representations of non-CO_2 forcings. This paper is organized as follows: in Sect. 2 we discuss the CAM GCM and our experimental design. In Sect. 3 we present the response to idealized stratospheric cooling and tropospheric heating, and compare these responses to a doubling of CO_2. Section 4 discusses the important physical mechanisms that explain most of the response. Conclusions follow in Sect. 5.

2 Methods

2.1 CAM description

The Community Atmosphere Model (CAM) version 3 (Collins et al., 2004), is the fifth generation of the National Center for Atmosphere Research (NCAR) atmospheric General Circulation Model (GCM) and is the atmospheric component of the Community Climate System Model (CCSM). CAM uses a Eulerian spectral transform dynamical core, where variables are represented in terms of coefficients of a truncated series of spherical harmonic functions. The model time step is 20-min, and time integration is performed with a semi-implicit leapfrog scheme. The vertical coordinate is a hybrid coordinate, with 26 vertical levels. The model has a relatively poorly-resolved stratosphere, with ~9 levels above 100 hPa and a top level at 2.9 hPa. The total parameterization package consists of four basic components: moist precipitation processes/convection, clouds and radiation, surface processes, and turbulent mixing. The land surface model is the Community Land Model (CLM) version 3 (Oleson et al., 2004), which combines realistic radiative, ecological and hydrologic processes.

ACPD
11, 31643–31688, 2011

2.2 Experimental design

CAM is run at T42 resolution (~ 2.8° × 2.8°) with a slab ocean-thermodynamic sea ice model. All experiments are run for at least 70 yr, the last 30 of which are used in this analysis, during which the model has reached equilibrium (i.e. no significant trend in TOA net energy flux).

Stratospheric cooling experiments (10PLO3; see Table 1) were performed by reducing the stratospheric ozone by 10 % globally, as well as individually for the tropics (±30°), mid-latitudes (30–60° N/S) and high-latitudes (60–90° N/S). The stratosphere is defined as the model levels above the tropopause, which is estimated by a thermal definition using the method of Reichler et al. (2003). We use CAM's default ozone boundary data set, which contains zonal monthly ozone volume mixing ratios, and reduce the ozone by 10 % at the appropriate latitudes and stratospheric pressures on a monthly basis. A 10 % ozone reduction is in rough agreement with the change in stratospheric ozone from 1979–2000 (Newchurch et al., 2003).

Our standard set of tropospheric heating experiments (LTHT) adds a 0.1 K day^{-1} (~3.5 W m^{-2}) heating source to the lower troposphere (surface to ~700 hPa). Such a heating rate is comparable to recent satellite-based estimates of present-day anthropogenic aerosol solar absorption (Chung et al., 2005). We conduct a globally uniform heating experiment, as well as latitudinally restricted heating of the tropics, mid- and high-latitudes. Although heating is only applied to the lower troposphere, the globally uniform temperature response resembles that based on a doubling of CO_2. This is due to destabilization of the lower atmosphere and increased convection, which vertically redistributes the heat throughout the depth of the troposphere. Similar experiments with mid-tropospheric and upper-tropospheric heating do not destabilize the lower atmosphere, and result in maximum tropospheric warming near the altitude of heat input. Table 2 lists the suite of tropospheric heating experiments. In all cases, the response is estimated as the difference between the experiment and a corresponding control, which lacks the added heat source.

ACPD
11, 31643–31688, 2011

A standard global warming experiment is also performed, where the CO_2 volume mixing ratio is doubled from 3.55×10^{-4} to 7.10×10^{-4}. We also conduct an extreme global warming experiment, where the CO_2 volume mixing ratio is increased by a factor of eight. The resulting climate signals are named $2 \times CO_2$ and $8 \times CO_2$, respectively.

Finally, our CAM integrations are compared to 12 2xCO2 CMIP3 equilibrium (slab ocean) experiments, as well as 10 1 % to 4xCO2 transient CMIP3 experiments. Table 3 lists the CMIP3 models used in this study. For the 1 % to 4xCO2 experiments, we compare the 25 years prior to CO_2 quadrupling (years 115–139) to the corresponding control.

2.3 Measures of tropical width and its changes

Several jet-based measures of tropical width were explored. This includes the latitude of the main jet, which we locate by finding the maximum of the zonally and monthly averaged zonal wind (U) in either hemisphere (NH or SH). The poleward jet displacements are then estimated by taking the difference of the mean jet location (experiment minus control) in either hemisphere. We computed this measure on each pressure level and averaged the 850–300 hPa displacements to obtain a tropospheric jet (TJ) displacement. Because our jet definition is based on the entire troposphere, it primarily represents the subtropical jet, and secondarily the mid-latitude eddy-driven jet. Displacements of the TJ and eddy-driven jet, however, are closely related; the correlation between 2xCO2 CMIP3 jet displacements using the annual mean 850–300 hPa U maximum and the near-surface (10-m) U maximum – which others have used as a measure of the eddy-driven jet (e.g. Kidston and Gerber, 2010) – is 0.83 in the NH and 0.90 in the SH. The correlation is weakest during JJA in the SH ($r = 0.57$), which is consistent with a winter-time decoupling of the subtropical and eddy jets, resulting in a double jet structure (e.g. Gallego et al., 2005).

We also investigated an additional method for locating the jet, where we located the "sides" of the jet and then found their midpoint; the sides were based on a specified percentile value of zonal wind. Although both methods yielded similar displacements,

ACPD
11, 31643–31688, 2011

testing indicated that the percentile method yielded somewhat more stable results; thus only the results from the percentile method, using the 75th percentile (p75), are shown. We do note, however, that the percentile method yields smaller displacements than the maximum method, and as the percentile is decreased (e.g. from 95 to 70), consistently smaller jet displacements are obtained. This is illustrated in Fig. 1, which compares tropospheric jet displacements in 12 CMIP3 2xCO2 equilibrium experiments using the maximum method, and the percentile method (with p75). A correlation of 0.95 shows both methods yields similar displacements; however, displacements tend to be larger with the jet maximum approach. The ensemble annual mean jet displacement using the maximum method is 0.62° in the NH and 0.96° in the SH; corresponding values using p75 are 0.46° and 0.73°. This result shows the jet displacement is non-uniform.

Figure 1 also shows the CMIP3 4xCO2 ensemble annual zonal mean tropospheric jet response, and the corresponding control. The response is not a uniform jet shift; there is some distortion of its shape, resulting in a poleward skew, which is larger for the faster winds. This is particularly evident in the SH, and helps to explain the larger poleward displacements with the jet maximum method. Similar, but weaker results exist for the 2xCO2 equilibrium experiments (not shown).

Additional measures of tropical displacement (Johanson and Fu, 2009) include (1) the latitude of the subtropical Mean Meridional Circulation (MMC) minima, defined as the latitudes where the MMC at 500 hPa becomes zero poleward of the subtropical maxima; and (2) the latitudes where precipitation minus evaporation ($P-E$) becomes zero on the poleward side of the subtropical minima (a measure of subtropical dry zone expansion). All displacements are estimated by first smoothing the zonal monthly mean of the appropriate model field(s) and interpolating to 0.5° resolution using cubic splines. Smoothing was performed by taking a running mean over ~10 degrees of latitude. Nearly identical results are obtained without interpolating.

In addition to zonal displacements, we also quantify the changes in the strength and altitude of the jet. The altitude of the jet was quantified by interpolating the zonal wind to 10 hPa vertical resolution, and locating the pressure of maximum monthly zonal wind.

ACPD
11, 31643–31688, 2011

This procedure is only done poleward of ∼20°, since the jet is not well defined in the tropics.

Throughout this manuscript, statistical significance is estimated with a standard t-test, using the pooled variance. The influence of serial correlation is accounted for by using the effective sample size, $n(1-\rho_1)(1+\rho_1)^{-1}$, where n is the number of years and ρ_1 is the lag-1 autocorrelation coefficient (Wilks, 1995).

3 Results

3.1 Responses to stratospheric cooling

3.1.1 Annual mean

Figure 2 shows the annual and zonal mean temperature and wind response for the stratospheric cooling (10PLO3) experiments. Also included is the meridional temperature gradient (T_y) response, with Southern Hemisphere (SH) T_y multiplied by −1 (and in all subsequent figures) so that negative T_y always represents colder air poleward. As expected, temperatures are generally colder, by ∼1 K, because of reduced solar absorption where the ozone reduction was imposed. Several non-local responses also occur, including tropospheric warming for the all-, high-, and mid-latitude experiments. These three experiments also yield an increase in zonal wind (U) near 60°, whose magnitude decays downward through the troposphere. This U increase occurs near the poleward flank of the tropospheric jet (TJ), while an opposite signed anomaly appears near the equatorward flank, indicating a poleward jet displacement. Note that reducing stratospheric ozone in the tropics ($10PLO3_{TR}$) yields the opposite response; however, the magnitude of the tropospheric wind anomaly is weak and not significant.

Table 4 quantifies the annual mean poleward displacement of the tropospheric (850–300 hPa) jets. As suggested by Fig. 2, stratospheric cooling generally yields a poleward displacement, of about 0.5° in each hemisphere. Cooling in the tropical stratosphere

ACPD
11, 31643–31688, 2011

yields the opposite, but the equatorward shift is small and not significant. Note that these changes are generally similar in both hemispheres, and across the four seasons. Furthermore, Table 5 shows the additional metrics of tropical displacement are generally consistent with the TJ response. For 10PLO3, $10PLO3_{HL}$ and $10PLO3_{ML}$, both $P-E$ and MMC yield annual mean poleward displacement, although smaller than that based on the tropospheric jet.

3.1.2 The springtime response and annular modes

To better understand the responses, we analyze more carefully in Figure 3 the March-April-May (MAM) responses of T, U and T_y to high-latitude cooling. This season shows the largest NH jet displacements (Table 4), and the equivalent season in the SH (SON) similarly shows the largest response in its jet. This is also generally true for the other metrics of tropical width, particularly in the SH during SON (not shown). The maximum spring response is likely due to a combination of two factors: the presence of solar radiation, so that the imposed ozone loss results in stratospheric cooling; and zonal flow conducive to strong planetary wave-mean flow interaction. Also included in Fig. 3 is the leading pattern of zonal wind anomalies, and the mean meridional circulation, associated with the NAM/SAM pattern. This pattern is based on a principal component analysis of geopotential heights for the domains extending from 20–90° N/S and from 1000 to 10 hPa. Data are weighted by the square root of the cosine of the latitude, as well as by the square root of the pressure interval represented by that level (Thompson and Wallace, 2000). The wind fields are then regressed upon the resulting standardized leading principal component (PC) time series.

The changes in zonal wind and mean meridional circulation closely resembles the NAM (and to a lesser extent, the SAM) pattern, which suggests the response may involve wave mean-flow interaction and downward control theory (Haynes et al., 1991; Baldwin and Dunkerton, 1999). The cooling of the high-latitude stratosphere increases the local meridional temperature gradient, and the stratospheric vortexes in both hemispheres intensify in accord with thermal wind balance. Refraction of Rossby waves is

ACPD
11, 31643–31688, 2011

governed by wind shear, among other factors, so that enhanced refraction occurs as the waves approach the positive wind anomaly (Shindell et al., 2001; Fletcher et al., 2007). Wave refraction is quantified as the ratio of meridional to vertical Eliassen Palm (EP) flux (Rind et al., 2005). Table 6 shows that all stratospheric cooling experiments–particularly 10PLO3$_{HL}$ – feature an increase in MAM NH wave refraction by 15–35 %. Figure 3 shows this is associated with an increases in equatorward and downward EP flux, and stratospheric/upper tropospheric wave divergence.

The MAM 10PLO3$_{HL}$ response also features an anomalous tropospheric meridional circulation, with rising motion poleward of 60°, sinking motion between 30–60°, and equatorward flow in the upper troposphere, somewhat like an intensified Ferrel Cell, but stretched poleward. This thermally indirect circulation coincides with warming near its sinking branch (near 45°), and cooling in the rising branch (near 70°). Imposition of these temperature anomalies on the background state produces a poleward displacement of the maximum tropospheric T_y, consistent with the tropospheric zonal wind anomaly near 60°. Figure 3 suggests that this anomalous residual circulation – particularly in the NH – is balanced by a poleward shift of eddy westerly momentum flux convergence near 60°, which sustains the westerly wind anomaly.

Table 4 also shows that the largest SH jet displacements (all poleward) occur during SON, which is the active season for the SAM. We find that our analysis of the NH spring-time response also approximately holds for the SH (not shown). For example, the SON zonal wind and mean meridional circulation responses closely resembles the SAM. Moreover, each experiment features an increase in wave refraction: 23 %, 21 %, 32 % and 2 % for 10PLO3, 10PLO3$_{HL}$, 10PLO3$_{ML}$ and 10PLO3$_{TR}$, respectively.

3.2 Response to tropospheric heating

3.2.1 Sensitivity to the latitudinal distribution of near-surface heating

Figure 4 shows the T, U and T_y response for the lower tropospheric heating experiments (LTHT). Similar to CO_2 forcing, globally uniform near-surface heating causes

ACPD
11, 31643–31688, 2011

a local warming maximum in the tropical upper troposphere due to moist convection, and high-latitude near-surface warming amplification due to snow and ice albedo feedbacks, as well as the higher static stability in polar regions. The zonal wind response to LTHT implies a poleward displacement of the NH tropospheric jet, but not the SH one. These shifts, however, are not statistically significant (see Table 4) in the annual mean or in any season.

Heating the individual latitude bands separately yields maximum warming at the heated latitudes, though with some spillover to most of the troposphere in the cases of $LTHT_{HL}$ and $LTHT_{ML}$. There are also some dynamically induced remote cooling responses, including significant stratospheric cooling for LTHT and weaker tropospheric high-latitude cooling for $LTHT_{TR}$.

A much stronger impact on tropical width occurs with heating restricted to midlatitudes than for the globally uniform case. $LTHT_{ML}$ shows both reduced U on the equatorward flank of the jet and increased U on the poleward jet flank, yielding significant poleward jet displacement of 0.66° in the NH and 1.02° in the SH. Significant displacements also occurred in experiments where either low or high latitudes were heated at the same time as mid-latitudes ($LTHT_{TRML}$ and $LTHT_{MLHL}$, respectively), supporting the robustness of this result. For example, Table 5 shows simultaneous heating of the low- and mid-latitudes yields a poleward jet displacement of 0.41° in the NH and 0.20° in the SH. $LTHT_{TRML}$ jet displacements become significant, and approximately double in magnitude, when the heating rate is doubled ($LTHT2x_{TRML}$).

Heating at high-latitudes ($LTHT_{HL}$) produced an opposite result, reducing U on the poleward TJ flank to produce an equatorward jet displacement of −0.42° over the two hemispheres, about a quarter of the poleward shift with midlatitude heating. Tropical heating ($LTHT_{TR}$) increased the peak U throughout the atmosphere, but without significantly shifting the jet position except upward. While the above conclusions are based on jet shifts, similar responses are found among other tropical displacement measures (Table 5), especially for the midlatitude heating which produced the strongest response.

ACPD
11, 31643–31688, 2011

Figure 5 shows the poleward displacement of the maximum meridional tropospheric temperature gradient for all experiments. $LTHT_{HL}$ yields equatorward displacement of the maximum T_y whereas $LTHT_{ML}$ features poleward displacement. This is consistent with the corresponding $LTHT_{HL}$ and $LTHT_{ML}$ tropospheric jet displacement – both quantities move poleward or equatorward together, in general agreement with thermal wind balance. For $LTHT_{ML}$, heating of the mid-latitudes weakens the temperature gradient on the equatorward flank of the maximum T_y, but increases it on the poleward flank, as shown in Fig. 4. The tropospheric jet then responds by shifting poleward. The opposite occurs for $LTHT_{HL}$. Small displacements of the maximum T_y generally occur for $LTHT_{TR}$, in agreement with the small TJ displacement.

We note that the changes during El Niño events are consistent with our results. El Niño is associated with tropical tropospheric warming by warmer Pacific SSTs, mid-latitude tropospheric cooling due to eddy-driven upward motion, and high-latitude tropospheric warming (Lu et al., 2008). The tropospheric jet, in turn, intensifies near the equatorward jet flank and weakens near the poleward flank, resulting in a strengthening and equatorward shift of the jet.

3.2.2 Evidence of nonlinear responses

Table 4 shows that the LTHT responses are similar, but generally larger, when the heating rate is doubled (LTHT2x). This includes tropical expansion for mid-latitude heating, tropical contraction for high-latitude heating, and negligible displacement for tropical heating. Unlike LTHT however, LTHT2x yields an overall equatorward TJ displacement of 0.61°, which is dominated by the SH, where the jet moves equatoward by 0.73°. Similarly, LTHT4x shows significant equatorward TJ displacement of 1.46°, which again is dominated by the SH jet.

The bottom panel of Fig. 5 shows that the relationship between displacements of the maximum meridional tropospheric temperature gradient and the tropospheric jet also applies for the LTHT2x experiments. Note that as the heating rate is increased and the tendency for TJ displacement is equatorward, the maximum T_y also shows a

ACPD
11, 31643–31688, 2011

similar tendency of equatorward displacement. LTHT4x, for example, shows significant equatorward displacement of the maximum T_y in both the SH and NH, in agreement with equatorward TJ displacement (Table 4), particularly in the SH.

One aspect of the uniform heating experiments that can be deduced from the above figures (e.g.Fig. 4) is that the responses are often nonlinear. For example, the sum of the poleward SH jet displacements in the $LTHT_{TR}$, $LTHT_{ML}$ and $LTHT_{HL}$ experiments is 0.77°, while the shift with uniform heating is smaller and in the opposite direction (−0.13°). This behavior recurs in the LTHT2x experiments, with values of 0.40° and −0.73° respectively. This nonlinear response is similar to the idealized experiments of Butler et al. (2010). This nonlinearity could be caused by the effects of localized heating on the vertical propagation of wave energy, and linear interference effects between the wave response and the background stationary wave (Smith et al., 2010; Fletcher and Kushner, 2011).

We note that such nonlinear jet displacements do not appear to occur in CMIP3 CO_2 experiments. Using the 10 4xCO2 CMIP3 models, we calculate the jet displacement using the 25 yr prior to doubling and the 25 yr prior to quadrupling (each compared to the corresponding control). For 4xCO2, the ensemble annual mean NH jet displacement is 0.98°, compared to 0.35° for 2xCO2; in the SH, the corresponding jet displacements are 1.74° and 0.81°, respectively. Thus, doubling the CO_2 forcing tends to yield double the jet displacement in CMIP3 experiments.

Nearly all of the CAM heating experiments, as well as 2xCO2, weaken the mean meridional circulation and strength of the tropospheric jet (not shown), in agreement with behavior of other GCMs and explainable by thermodynamic arguments (Held and Soden, 2006). $LTHT_{TR}$, however, strengthens the tropical circulation, with a 2 % increase in TJ jet strength and a 4 % increase in mean meridional circulation strength. This strengthening increases to 5 % and 7 %, respectively, for $LTHT2X_{TR}$, so this particular result is relatively linear. These latitudinally restricted heating responses are consistent with thermal wind balance. For example, low-latitude heating results in tropical warming, which reinforces the climatological meridional temperature gradient (T_y). This

ACPD
11, 31643–31688, 2011

implies an increase in upper level westerlies by thermal wind balance, in proportion to the amount of tropical warming. Heating off the equator weakens the climatological T_y and yields a weaker tropical circulation.

3.3 Comparison of greenhouse gas warming and lower-tropospheric heating

Figure 6 shows the annual mean T and U response for LTHT and 2xCO2. Both feature similar patterns of warming, with maximum warming in the tropical upper troposphere and at high-latitudes. Both also feature an increase in the height of the tropopause, as well as an upward displacement of the tropospheric jets (~10 hPa for 2xCO2 and ~5 hPa for LTHT), which generally occurs with tropospheric heating (e.g. Lorenz and DeWeaver, 2007). The zonal jet displacement is also similar for the two experiments, with small SH displacements and larger NH poleward displacements, the latter of which is reminiscent of the positive NAM pattern. Note that the LTHT signal is much weaker than 2xCO2. However, the global annual mean surface temperature response for LTHT is also much weaker: 0.91 K versus 2.52 K for 2xCO2.

For 2xCO2 and LTHT, Table 4 shows NH tropical expansion primarily occurs during two seasons: MAM and DJF. Figure 7 shows the MAM U response, which is characterized by a NAM-like U and meridional circulation response pattern. Similar to the high-latitude ozone depletion experiment previously discussed, this response is associated with wave-mean flow interaction. Both signals feature an increase in wave refraction (Table 6), which is associated with an increase in downward, equatorward wave energy and EP-flux divergence in the mid-latitude stratosphere and troposphere. The anomalous meridional circulation in the troposphere features rising motion near 70° N and sinking motion near 50° N, with equatorward flow in the upper troposphere. This anomalous circulation is balanced by a poleward shift of eddy westerly momentum flux convergence near 60° N, which sustains the westerly wind anomaly. This suggests that in addition to perturbed tropospheric temperature gradients, wave-mean flow interaction may play an important role in warming induced tropical expansion, particularly in the NH during MAM and DJF, regardless of the cause of the warming. Similar behavior

ACPD
11, 31643–31688, 2011

occurs in the extreme global warming experiment, 8xCO2, as well as in the mid-latitude lower-tropospheric heating experiment. For example, LTHT2x$_{ML}$ features a DJF/MAM increase in downward, equatorward wave energy (increase in wave refraction, Table 6) and EP-flux divergence, as well as cooling of the polar stratosphere, and a decrease in polar stratospheric geopotential heights (not shown). Thus, the tropospheric heating pathway also involves the wave-modulated stratospheric pathway. This is consistent with the positive Arctic Oscillation type response to anthropogenic aerosols found by Allen and Sherwood (2011).

Our experiments from Sect. 3.1 show that stratospheric cooling causes poleward TJ displacement. Therefore, one reason why the LTHT experiments may yield less poleward TJ displacement than those of 2xCO2, is because 2xCO2 is associated with significant stratospheric cooling due to increased longwave emission to space; LTHT, however, has no directly imposed stratospheric cooling (although there is an indirect stratospheric cooling response). This was evaluated by rerunning the LTHT, LTHT2x and LTHT4x experiments, but with a 10 % stratospheric ozone reduction. For both LTHT2x and LTHT4x, adding stratospheric cooling yields less equatorward TJ displacement, particularly in the SH, but the differences are not large (∼25 % less equatorward displacement for LTHT4x). This suggests the tropospheric warming is of primary importance.

4 Discussion of expansion mechanisms

Most prior studies have attributed tropical expansion in a warmer climate to increases in the tropopause height (e.g. Lorenz and DeWeaver, 2007) and/or extratropical dry static stability (e.g. Frierson et al., 2007; Lu et al., 2007). Figure 8 shows the changes in these two quantities, in addition to the 500 hPa T_y change and its climatology for four of the tropospheric heating experiments. These four experiments were chosen because they allow the evaluation of these previously proposed mechanisms. The top two panels compare the response based on heating of the mid-latitudes in either the lower (LTHT$_{ML}$) or upper (UTHT$_{ML}$) troposphere. Of the two, the latter results in a

ACPD
11, 31643–31688, 2011

larger increase in gross dry static stability of mid-latitudes, as expected. Although both experiments yield poleward TJ displacement, tropical expansion is generally larger with $LTHT_{ML}$. Table 4 shows this is particularly true in the SH, where the annual mean jet displacement is 1.02° for $LTHT_{ML}$ versus 0.53° for $UTHT_{ML}$. Similar conclusions exist based on the other metrics of tropical expansion (Table 5), particularly $P-E$. The larger $LTHT_{ML}$ poleward TJ displacement is inconsistent with a smaller increase in stability; however, it is consistent with thermal wind balance and a larger poleward displacement of the 500 hPa SH T_y.

The bottom two panels show that heating of the high-latitudes and tropics results in an increase in tropopause height (decrease in pressure), yet neither experiment is associated with tropical expansion. $LTHT2x_{HL}$ actually yields significant equatorward TJ displacement of −0.74° (−0.32° and −0.42° for NH and SH, respectively) and $LTHT2x_{TR}$ yields negligible jet displacement of −0.23° (Table 4). These responses are again consistent with the change in T_y at 500 hPa, with a weakening of T_y at high latitudes for $LTHT2x_{HL}$, and a reinforcement of the climatological T_y for $LTHT2x_{TR}$. These results suggest the importance of other mechanisms in driving TJ displacements, at least using CAM under our experimental design.

Figure 9 shows a scatterplot of the tropospheric (850–300 hPa) jet displacement versus the difference between mid-latitude and high-latitude warming amplification for the global warming experiments (LTHT, LTHT2x, LTHT4x, 2xCO2 and 8xCO2). Warming amplification of mid-latitudes (AMP_{ML}) is defined as the log-pressure area weighted temperature (i.e. thickness) response between 30–60° minus that between 0–30°. For high-latitudes (AMP_{HL}), the log-pressure area weighted temperature response between 60–90° is differenced with that between 30–60°. Table 7 lists the amplification factors. This choice of this metric was inspired by the responses found in the latitude-restricted tropospheric heating experiments. When high-latitudes warm relative to mid-latitudes, AMP_{HL} is positive, and we expect equatorward jet displacement. When the mid-latitudes warm relative to low-latitudes, AMP_{ML} is positive, and we expect poleward jet displacement. Taking the difference, $AMP_{ML}-AMP_{HL}$, results

ACPD
11, 31643–31688, 2011

in a quantity that accounts for these two competing effects. As the difference becomes more positive/less negative, then mid-latitude warming amplification dominates, and we expect more tropical expansion/less contraction; vice versa as $AMP_{ML} - AMP_{HL}$ becomes less positive/more negative. We call this quantity the "Expansion Index" (EI).

The global warming experiments are generally consistent with this notion. Over all five experiments and seasons, the relationship is significant at the 99 % confidence level for NH, SH and both hemispheres, accounting for 42 %, 72 % and 55 % of the TJ displacement, respectively. For the annual mean only, the expansion index accounts for 76 % of the NH and SH jet displacement. The dominant response in these experiments – equatorward SH jet displacement – is consistent with the large SH high-latitude warming, and large AMP_{HL}. The diagnostic also explains the increased equatorward displacement when the heating rate is increased in the LTHT experiments. Increasing the heating rate generally results in amplified high-latitude warming, which is associated with equatoward jet displacement. Table 7 shows that the annual mean SH AMP_{HL} increases from 0.22 to 1.02 K for LTHT to LTHT4x; and from 0.02 to 0.64 K in the NH. At the same time, however, AMP_{ML} generally decreases, particularly in the NH. Furthermore, AMP_{HL} is generally largest in the SH, relative to the NH, consistent with equatorward SH jet displacement in nearly all cases. The relationship is weakest in the NH for DJF and MAM, but this is consistent with the important role of wave-mean flow interaction during these seasons, which are the active seasons for NH troposphere-stratosphere coupling. Without DJF and MAM, the expansion index accounts for 81 % of the variation in NH TJ displacement. Similar conclusions exist when the three mid-tropospheric global warming experiments (MTHT, MTHT2x and MTHT4x) are included in the analysis.

Figure 9 further supports the idea that part of the jet shift can be thought of as a geostrophic adjustment to an altered temperature profile – not only when certain latitude bands are heated, but also for global warming experiments like LTHT and 2xCO2. Our experiments suggest that TJ poleward displacement is partially driven by mid-latitude heating, while TJ equatorward displacement is partially driven by

ACPD
11, 31643–31688, 2011

high-latitude heating. However, wave-mean flow interaction during the NH active seasons is also important, resulting in poleward NH jet displacement during MAM and DJF which projects onto the positive phase of the NAM. For LTHT this mechanism eventually weakens with increased heating (e.g. LTHT4x), where high-latitude amplification dominates and the maximum T_y is displaced equatorward, resulting in equatorward displacement of the tropospheric jets.

Figure 9 also shows a similar relationship between the expansion index and TJ displacement exist based on CMIP3 2xCO2 equilibrium experiments. Even though this metric does not directly account for the effects of CO_2 induced stratospheric cooling, it accounts for 45 %, 67 % and 56 % of the of the variation in TJ displacement in the NH, SH and both hemispheres, respectively. Based on the annual mean only, EI accounts for 76 % of the NH and SH jet displacement. Similar results are obtained if jet displacements are based on others percentiles. Using the 70th–95th percentile in 5 percentile increments, EI accounts for 61 % to 77 % of the annual mean jet displacement; using the alternate, maximum U method, 66 % of the annual mean TJ displacement is accounted for. This relationship is somewhat better than the relationship Lu et al. (2007) found between tropical expansion and tropopause height (stability); there, increases in extratropical (35–55°) tropopause height accounted for 66 % of the variation in annual mean MMC expansion using CMIP3 A2 experiments. More recently, Lu et al. (2008) found a significant relationship between poleward MMC displacement and a decrease in Philips criticality, the latter of which occurred primarily due to an increase in extratropical static stability. In the SH during DJF, Philips criticality accounted for 67 % of the variation in MMC expansion. Similarly, the expansion index accounts for 92 % of the TJ displacement in the SH during DJF. We also find that it accounts for most of the DJF SH variation in other metrics of tropical expansion, including $P-E$ (81 %) and MMC (81 %). Similar, but weaker, results exist for SH ANN, where the expansion index accounts for 45 % and 46 % of the variation in $P-E$ and MMC, respectively. Thus, the expansion index helps to explain not only dynamical measures of tropical expansion, but hydrological measures too, particularly in the SH.

ACPD
11, 31643–31688, 2011

We also estimated the relationship between the expansion index and tropospheric jet displacement using the 10 1 % to 4xCO2 CMIP3 experiments, and with five reanalyses, including NCEP/NCAR (Kalnay et al., 1996), NCEP-DOE (Kanamitsu et al., 2002), MERRA (Rienecker et al., 2011), ERA40 (Uppala et al., 2005) and ERA-Interim (Dee et al., 2011). The first three reanalyses are analyzed from 1979–2010; ERA40 from 1979–2002 and ERA-Interim from 1989–2010. Based on the annual mean, the expansion index accounts for 70 % of the variance in NH and SH jet displacements in 4xCO2 CMIP3 experiments; and 55 % of the corresponding jet displacements in reanalyses.

We conclude by comparing the CAM global warming experiments with the CMIP3 2xCO2 experiments. Similar to the CAM experiments, the EI-jet displacement relationship is weakest in the NH during DJF, where it accounts for only 46 % of the variation in TJ displacement. However, CMIP3 also features an increase in NH DJF wave refraction (13 %; Table 6), supporting the notion wave-mean flow interaction is important during boreal winter. Furthermore, a significant, but weak, relationship exists between CMIP3 NH DJF wave refraction and jet displacement, with a correlation of 0.44. Wave-mean flow interaction is also important in the NH during MAM, where the CMIP3 correlation between wave refraction and jet displacement is 0.43. We also note that the NH MAM CAM 2xCO2 jet displacement is much larger than the CMIP3 ensemble (Table 4), which is consistent with more MAM wave refraction in CAM 2xCO2 (56 % versus the CMIP3 ensemble mean of 15 %). CAM 2xCO2 also features less SH jet displacement than CMIP3 (0.09° versus 0.73° for the annual mean), despite a similar expansion index (−0.14 versus −0.18 for CMIP3). Although the reasons are not clear, the other metrics of CAM 2xCO2 tropical width both show greater SH displacement (0.60° for $P-E$ and 0.42° for MMC).

5 Conclusions

The CAM3 general circulation model is used to investigate how tropical width responds to idealized thermal perturbations, focusing on zonal displacement of the tropospheric

ACPD
11, 31643–31688, 2011

jets (TJs). The heat sources include global and zonally restricted lower-tropospheric warmings and stratospheric coolings, which coarsely represent possible impacts of ozone or aerosol changes. Our results show that global stratospheric cooling, as well as stratospheric cooling of the high- and mid-latitudes, yields poleward TJ displacement. This response is related to wave-mean flow interaction and involves an increase in wave refraction, and downward propagation of the stratospheric wind anomaly. This response is in general agreement with similar studies using idealized models (e.g. Haigh et al., 2005) and supports the recent findings of Polvani et al. (2011), who showed stratospheric ozone loss is the main driver of twentieth century atmospheric circulation changes in the Southern Hemisphere (SH).

CAM3 tropospheric heating experiments show that high-latitude heating results in equatorward jet displacement; mid-latitude heating results in poleward jet displacement; and low-latitude heating yields negligible TJ displacement (but a significant increase in the strength of the tropical circulation). Although our high-latitude response is consistent with a recent study using a simplified GCM (Butler et al., 2010), our tropical heating results differ – Butler et al. (2010) found tropical heating forces a significant poleward shift of the extratropical storm tracks (and tropospheric jets). We note that the Butler et al. (2010) results appear to contradict the El Ninõ response, which is associated with tropical tropospheric warming and equatorward displacement of the jets (Lu et al., 2008). Reasons for this discrepancy are unclear, but may be related to the altitude of the imposed heating. Butler et al. (2010) added heat to the tropical upper troposphere ($UTHT_{TR}$), whereas our experiments feature lower-tropospheric heating. We do note that the tropical mid-troposphere heating experiment of Butler et al. (2010) yielded a smaller poleward storm track shift compared to their $UTHT_{TR}$ experiments. Similarly, our $MTHT2x_{TR}$ experiment yielded more poleward/less equatorward displacement that $LTHT2x_{TR}$ (as did MTHT2x versus LTHT2x; Table 5). This implies elevated heating of the tropical troposphere – where the meridional temperature gradient is largest – yields greater poleward displacement of the jets. Such a response is consistent with the mechanism of Chen and Held (2007) and Chen et al. (2008), who

ACPD
11, 31643–31688, 2011

argue the enhanced upper-tropospheric meridional temperature gradient is associated with enhanced westerlies and Rossby waves with increased phase speed, which break at anomalously poleward latitudes.

Globally uniform lower tropospheric heating (LTHT) and 2xCO2 yield similar tropical width responses. Both yield negligible TJ displacement in the SH and poleward TJ displacement in the NH, particularly during DJF and MAM. Similar to the stratospheric cooling experiments, the boreal winter/spring expansion is related to wave mean flow interaction and a positive NAM-like response. This result is consistent with Previdi and Liepert (2007), who showed 50 % of the subtropical dry zone expansion can be explained by positive trends in the annular modes. Other metrics of tropical displacement, including $P-E$ and MMC, generally yield a similar response. However, there are some differences that warrant further study.

Jet shifts associated with the tropospheric heating experiments are related to zonal displacements of the maximum meridional tropospheric temperature gradient. Heating the mid-latitudes results in maximum mid-latitude warming, which weakens the tropospheric meridional temperature gradient (T_y) on the equatorward flank of the T_y maximum and strengthens T_y on the poleward flank of the maximum. The jet responds by moving poleward, consistent with thermal wind balance. The opposite occurs when heat is added to the high-latitudes. This relationship also exists for global warming experiments, including LTHT and 2xCO2.

Some of our experiments are inconsistent with previously proposed mechanisms of tropical expansion (e.g. Lorenz and DeWeaver, 2007; Frierson et al., 2007; Lu et al., 2007). For example, heating the tropical troposphere results in a global increase in tropopause height, yet negligible poleward tropical displacement. Our experiments highlight the importance of altered tropospheric temperature gradients and wave-mean flow interaction. For the global warming experiments, the "Expansion Index", which quantifies the difference between mid-latitude and high-latitude warming amplification, accounts for over half of the tropospheric jet displacements; this increases to over 70 % for annual mean jet displacements. A similar relationship also exists for 2xCO2

ACPD
11, 31643–31688, 2011

CMIP3 equilibrium experiments and 1 % to 4xCO2 CMIP3 transient experiments. Five reanalyses also show the relationship exists for recent climate trends.

This study has important implications for heterogeneous warming agents, such as tropospheric ozone and absorbing aerosols, as briefly discussed by Allen and Sherwood (2011). Such non-CO_2 forcings – particularly those that warm the mid-latitudes and are underestimated by most models (e.g. Ramanathan and Carmichael, 2008; Koch et al., 2009) – may help explain the discrepancy between modeled and observed estimates of recent tropical expansion. Moreover, a recent study by Scaife et al. (2011) found increased CO_2 in GCMs with a well-resolved stratosphere yielded an equatorward storm track shift, particularly over the Atlantic during winter. This implies the observed poleward shift may be due more to heterogeneous warming agents, as opposed to greenhouse gases. We are currently investigating the importance of non-CO_2 forcings in recent tropical expansion.

Acknowledgements. This study was funded by RJA's UCR initial complement, SIO NOAA grant NA10OAR43210141, and by NSF ARC-0714088 and NASA NNX07AR23G, UC Irvine. We acknowledge the modeling groups, the Program for Climate Model Diagnosis and Intercomparison (PCMDI) and the WCRP's Working Group on Coupled Modelling (WGCM) for their roles in making available the WCRP CMIP3 multi-model dataset. Support of this dataset is provided by the Office of Science, US Department of Energy.

References

Allen, R. J. and Sherwood, S. C.: The impact of natural versus anthropogenic aerosols on atmospheric circulation in the Community Atmosphere Model, Climate Dyn., 36, 1959–1978, 2011. 31659, 31666

Baldwin, M. P. and Dunkerton, T. J.: Propagation of the Arctic Oscillation from the stratosphere to the troposphere. J. Geophys. Res., 104, 30937–30946, 1999. 31653

Bond, T. C., Bhardwaj, E., Dong, R., Jogani, R., Jung, S., Roden, C., Streets, D. G., and Trautmann, N. M.: Historical emissions of black and organic carbon aerosol from energy related

ACPD
11, 31643–31688, 2011

combustion, 1850–2000, Glob. Biogeochem. Cy., 21, GB2018, doi:10.1029/2006GB002840, 2007. 31647

Butler, A. H., Thompson, D. W. J., and Heikes, R.: The steady-state atmospheric circulation response to climate change-like thermal forcings in a simple general circulation model, J. Climate, 23, 3474–3496, 2010. 31647, 31657, 31664

Butler, A. H., Thompson, D. W. J., and Birner, T.: Isentropic slopes, downgradient eddy fluxes, and the extratropical atmospheric circulation response to tropical tropospheric heating, J. Atmos. Sci., 68, 2292–2305, 2011. 31647

Chen, G. and Held, I.: Phase speed spectra and the recent poleward shift of the Southern Hemisphere surface westerlies, Geophys. Res. Lett., 34, L21805, doi:10.1029/2007GL031200, 2007. 31647, 31664

Chen, G., Lu, J., and Frierson, D. W.: Phase speed spectra and the latitude of surface westerlies: Interannual variability and global warming trend, J. Climate, 21, 5942–5959, 2008. 31647, 31664

Chung, C. E., Ramanathan, V., Kim, D., and Podgorny, I. A.: Global anthropogenic aerosol direct forcing derived from satellite and ground-based observations, J. Geophys. Res., 110, D24207, doi:10.1029/2005JD006356, 2005. 31649

Collins, W. D., Rasch, P. J., Boville, B. A., Hack, J. J., McCaa, J. R., Williamson, D. L., Kiehl, J. T., Briegleb, B., Bitz, C., Lin, S.-J., Zhang, M., and Dai, Y.: Description of the NCAR Community Atmosphere Model (CAM 3.0), Technical Report NCAR/TN-464+STR, National Center for Atmospheric Research, Boulder, CO, 226 pp., 2004. 31648

Dee, D. P., Uppala, S. M., Simmons, A. J., Berrisford, P., Poli, P., Kobayashi, S., Andrae, U., Balmaseda, M. A., Balsamo, G., Bauer, P., Bechtold, P., Beljaars, A. C. M., van de Berg, L., Bidlot, J., Bormann, N., Delsol, C., Dragani, R., Fuentes, M., Geer, A. J., Haimberger, L., Healy, S. B., Hersbach, H., Hólm, E. V., Isaksen, L., Kållberg, P., Köhler, M., Matricardi, M., McNally, A. P., Monge-Sanz, B. M., Morcrette, J.-J., Park, B.-K., Peubey, C., de Rosnay, P., Tavolato, C., Thépaut, J.-N., and Vitart, F.: The ERA-Interim reanalysis: Configuration and performance of the data assimilation system, Q. J. Roy. Meteorol. Soc., 137, 553–597, 2011. 31663

Fletcher, C. G. and Kushner, P. J.: The role of linear interference in the Annular Mode response to Tropical SST forcing, 24, 778–794, J. Climate, doi:10.1175/2010JCLI3735.1, 2011. 31657

Fletcher, C. G., Kushner, P. J., and Cohen, J.: Stratospheric control of the extratropcial circulation response to surface forcing, Geophys. Res. Lett., 34, L21802,

ACPD
11, 31643–31688, 2011

doi:10.1029/2007GL031626, 2007. 31654
Frierson, D. M. W., Lu, J., and Chen, G.: Width of the Hadley cell in simple and comprehensive general circulation models, Geophys. Res. Lett., 34, L18804, doi:10.1029/2007GL031115, 2007. 31646, 31659, 31665
Fu, Q. and Lin, P.: Poleward shift of subtropical jets inferred from satellite-observed lower stratospheric temperatures. J. Climate, 24, 5597–5603, doi:10.1175/JCLI-D-11-00027.1, 2011. 31645
Fu, Q., Johanson, C. M., Wallace, J. M., and Reichler, T.: Enhanced mid-latitude tropospheric warming in satellite measurements. Science, 312, 1179, doi:10.1126/science.1125566, 2006. 31645
Gallego, D., Ribera, P., Garcia-Herrera, R., Hernandez, E., and Gimeno, L.: A new look for the Southern Hemisphere jet stream. Climate Dyn., 24, 607–621, 2005. 31650
Haigh, J. D., Blackburn, M., and Day, R.: The response of tropopsheric circulation to perturbations in lower-stratospheric temperature, J. Climate, 18, 3672–3685, 2005. 31646, 31664
Haynes, P. H., Marks, C. J., McIntyre, M. E., Shepherd, T. G., and Shine, K. P.: On the "downward control" of extratropical diabatic circulations by eddy-induced mean zonal forces, J. Atmos. Sci., 48, 651–678, 1991. 31653
Held, I. M.: The general circulation of the atmosphere, paper presented at 2000 Woods Hole Oceanographic Institute Geophysical Fluid Dynamics Program. Woods Hole Oceanographic Institute, Woods Hole, Mass, available at: http://www.whoi.edu/page.do?pid=13076, 2000. 31646
Held, I. M. and Soden, B. J.: Robust responses of the hydrological cycle to global warming, J. Climate, 19, 5686–5699, 2006. 31657
Hu, Y. and Fu, Q.: Observed poleward expansion of the Hadley circulation since 1979, Atmos. Chem. Phys., 7, 5229–5236, doi:10.5194/acp-7-5229-2007, 2007. 31644
Hudson, R. D., Andrade, M. F., Follette, M. B., and Frolov, A. D.: The total ozone field separated into meteorological regimes – Part II: Northern Hemisphere mid-latitude total ozone trends, Atmos. Chem. Phys., 6, 5183–5191, doi:10.5194/acp-6-5183-2006, 2006. 31645
Johanson, C. M. and Fu, Q.: Hadley cell widening: Model simulations versus observations, J. Climate, 22, 2713–2725, 2009. 31645, 31651
Kalnay, E., Kanamitsu, M., Kistler, R., Collins, W., Deaven, D., Gandin, L., Iredell, M., Saha, S., White, G., Woollen, J., Zhu, Y., Leetmaa, A., Reynolds, B., Chelliah, M., Ebisuzaki, W., Higgins, W., Janowiak, J., Mo, K. C., Ropelewski, C., Wang, J., Jenne, R., and Hoseph, D.:

ACPD
11, 31643–31688, 2011

The NCEP/NCAR 40-year reanalysis project, B. Am. Meteorol. Soc., 77, 437–471, 1996. 31663

Kanamitsu, M., Ebisuzaki, W., Woollen, J., Yang, S.-K., Hnilo, J. J., Fiorino, M., and Potter, G. L.: NCEP-DOE AMIP-II Reanalysis (R-2), B. Am. Meteor. Soc., 83, 1631–1643, 2002. 31663

Kidston, J. and Gerber, E. P.: Intermodel variability of the poleward shift of the austral jet stream in the CMIP3 integrations linked to biases in 20th century climatology, Geophys. Res. Lett., 37, L09708, doi:10.1029/2010GL042873, 2010. 31650

Kidston, J., Dean, S. M., Renwick, J. A., and Vallis, G. K.: A robust increase in the eddy length scale in the simulation of future climates, Geophys. Res. Lett., 37, L03806, doi:10.1029/2009GL041615, 2010. 31647

Kidston, J., Vallis, G. K., Dean, S. M., and Renwick, J. A.: Can the increase in the eddy length scale under global warming cause the poleward shift of the jet streams?, J. Climate, 24, 3764–3780, doi:10.1175/2010JCLI3738.1, 2011. 31647

Koch, D., Schulz, M., Kinne, S., McNaughton, C., Spackman, J. R., Balkanski, Y., Bauer, S., Berntsen, T., Bond, T. C., Boucher, O., Chin, M., Clarke, A., De Luca, N., Dentener, F., Diehl, T., Dubovik, O., Easter, R., Fahey, D. W., Feichter, J., Fillmore, D., Freitag, S., Ghan, S., Ginoux, P., Gong, S., Horowitz, L., Iversen, T., Kirkevåg, A., Klimont, Z., Kondo, Y., Krol, M., Liu, X., Miller, R., Montanaro, V., Moteki, N., Myhre, G., Penner, J. E., Perlwitz, J., Pitari, G., Reddy, S., Sahu, L., Sakamoto, H., Schuster, G., Schwarz, J. P., Seland, Ø., Stier, P., Takegawa, N., Takemura, T., Textor, C., van Aardenne, J. A., and Zhao, Y.: Evaluation of black carbon estimations in global aerosol models, Atmos. Chem. Phys., 9, 9001–9026, doi:10.5194/acp-9-9001-2009, 2009. 31666

Kushner, P. J. and Polvani, L. M. (2004). Stratosphere-troposphere coupling in a relatively simple AGCM: The role of eddies, J. Climate, 17, 629–639, 2004. 31646

Kushner, P. J., Held, I. M., and Delworth, T. L.: Southern Hemisphere atmospheric circulation response to global warming, J. Climate, 14, 2238–2249, 2001. 31645

Lorenz, D. J. and DeWeaver, E. T.: Tropopause height and zonal wind response to global warming in the IPCC scenario integrations, J. Geophys. Res., 112, D10119, doi:10.1029/2006JD008087, 2007. 31645, 31646, 31658, 31659, 31665

Lu, J., Vecchi, G. A., and Reichler, T.: Expansion of the Hadley cell under global warming, Geophys. Res. Lett., 34, L06805, doi:10.1029/2006GL028443, 2007. 31645, 31659, 31662, 31665

ACPD
11, 31643–31688, 2011

Lu, J., Chen, G., and Frierson, D. M. W.: Response of the zonal mean atmospheric circulation to El Niño versus global warming, J. Climate, 21, 5835–5851, 2008. 31646, 31656, 31662, 31664

Lu, J., Deser, C., and Reichler, T.: Cause of the widening of the tropical belt since 1958, Geophys. Res. Lett., 36, L03803, doi:10.1029/2008GL036076, 2009. 31645

Newchurch, M. J., Yang, E.-S., Cunnold, D. M., Reinsel, G. C., Zawodny, J. M., and RussellIII, J. M.: Evidence for slowdown in stratospheric ozone loss: First stage of ozone recovery, J. Geophys. Res., 108, 4507, doi:10.1029/2003JD003471, 2003. 31649

Oleson, K. W., Dai, Y., Bonan, G., Bosilovich, M., Dickinson, R., Dirmeyer, P., Hoffman, F., Houser, P., Levis, S., Niu, G.-Y., Thornton, P., Vertenstein, M., Yang, Z.-L., and Zeng, X.: Technical description of the Community Land Model (CLM). Technical Report NCAR/TN-461+STR, National Center for Atmospheric Research, Boulder, CO, 174 pp., 2004. 31648

Polvani, L. M. and Kushner, P. J.: Tropospheric response to stratospheric perturbations in a relatively simple general circulation model, Geophys. Res. Lett., 29, 1114, doi:10.1029/2001GL014284, 2002. 31646

Polvani, L. M., Waugh, D. W., Correa, G. J. P., and Son, S.-W.: Stratospheric ozone depletion: The main driver of twentieth-century atmospheric circulation changes in the Southern Hemisphere, J. Climate, 24, 795–812, 2011. 31646, 31664

Previdi, M. and Liepert, B. G.: Annular modes and Hadley cell expansion under global warming, Geophys. Res. Lett., 34, L22701, doi:10.1029/2007GL031243, 2007. 31645, 31665

Ramanathan, V. and Carmichael, G.: Global and regional climate changes due to black carbon, Nature Geosci., 1, 221–227, 2008. 31666

Reichler, T., Dameris, M., and Sausen, R.: Determining the tropopause height from gridded data, Geophys. Res. Lett., 30, 2042, doi:10.1029/2003GL018240, 2003. 31649

Rienecker, M. M., Suarez, M. J., Gelaro, R., Todling, R., Bacmeister, J., Liu, E., Bosilovich, M. G., Schubert, S. D., Takacs, L., Kim, G.-K., Bloom, S., Chen, J., Collins, D., Conaty, A., da Silva, A., Gu, W., Joiner, J., Koster, R. D., Lucchesi, R., Molod, A., Owens, T., Pawson, S., Pegion, P., Redder, C. R., Reichle, R., Robertson, F. R., Ruddick, A. G., Sienkiewicz, M., and Woollen, J.: MERRA: NASA's Modern-Era Retrospective Analysis for Research and Applications, J. Climate, 24, 3624–3648, 2011. 31663

Rind, D., Perlwitz, J., and Lonergan, P.: AO/NAO response to climate change: 1. Respective influences of stratospheric and tropospheric climate changes, J. Geophys. Res., 110, D12107, doi:10.1029/2004JD005103, 2005. 31654

ACPD
11, 31643–31688, 2011

Scaife, A., Spangehl, T., Fereday, D., Cubasch, U., Langematz, U., Akiyoshi, H., Bekki, S., Braesicke, P., Butchart, N., Chipperfield, M., Gettelman, A., Hardiman, S., Michou, M., Rozanov, E., and Shepherd, T.: Climate change projections and stratosphere–troposphere interaction, Climate Dyn., doi:10.1007/s00382-011-1080-7, in press, 2011. 31666

Seidel, D. J. and Randel, W. J.: Recent widening of the tropical belt: Evidence from tropopause observations, J. Geophys. Res., 112, D20113, doi:10.1029/2007JD008861, 2007. 31645

Seidel, D. J., Fu, Q., Randel, W. J., and Reichler, T. J.: Widening of the tropical belt in a changing climate, Nature Geosci., 1, 21–24, doi:10.1038/ngeo.2007.38, 2008. 31644

Shindell, D. T., Schmidt, G. A., Miller, R. L., and Rind, D.: Northern Hemisphere winter climate response to greenhouse gas, ozone, solar, and volcanic forcing, J. Geophys. Res., 106, 7193–7210, 2001. 31654

Shindell, D. T., Faluvegi, G., Lacis, A., Hansen, J., Ruedy, R., and Aguilar, E.: Role of tropospheric ozone increases in 20th-century climate change, J. Geophys. Res., 111, D08302, doi:10.1029/2005JD006348, 2006. 31647

Smith, K. L., Fletcher, C. G., and Kushner, P. J.: The role of linear interference in the Annular Mode response to extratropical surface forcing, J. Climate, 23, 6036–6050, 2010. 31657

Smith, S. J., van Aardenne, J., Klimont, Z., Andres, R. J., Volke, A., and Delgado Arias, S.: Anthropogenic sulfur dioxide emissions: 1850–2005, Atmos. Chem. Phys., 11, 1101–1116, doi:10.5194/acp-11-1101-2011, 2011. 31647

Thompson, D. W. J. and Wallace, J. M.: Annular modes in the extratropical circulation. Part I: Month to month variability, J. Climate, 13, 1000–1016, 2000. 31653

Uppala, S., Kallberg, P., Simmons, A., Andrae, U., Bechtold, V., Fiorino, M., Gibson, J., Haseler, J., Hernandez, A., Kelly, G., Li, X., Onogi, K., Saarinen, S., Sokka, N., Allan, R., Andersson, E., Arpe, K., Balmaseda, M., Beljaars, A., Van De Berg, L., Bidlot, J., Bormann, N., Caires, S., Chevallier, F., Dethof, A., Dragosavac, M., Fisher, M., Fuentes, M., Hagemann, S., Holm, E., Hoskins, B., Isaksen, L., Janssen, P., Jenne, R., McNally, A., Mahfouf, J., Morcrette, J., Rayner, N., Saunders, R., Simon, P., Sterl, A., Trenberth, K., Untch, A., Vasiljevic, D., Viterbo, P., and Woollen, J.: The ERA-40 re-analysis, Q. J. Roy. Meteorol. Soc., 131, 2961–3012, 2005. 31663

van Aardenne, J. A., Dentener, F. J., Olivier, J. G. J., Goldewijk, C. G. M. K., and Lelieveld, J.: A 1 x 1 degree resolution dataset of historical anthropogenic trace gas emissions for the period 1890–1990, Global. Biogeochem. Cy., 15, 909–928, 2001. 31647

Wang, S., Gerber, E. P., and Polvani, L. M.: Abrupt circulation responses to tropical upper tropo-

ACPD
11, 31643–31688, 2011

spheric warming in a relatively simple stratosphere-resolving AGCM, J. Climate, submitted, 2011. 31647

Wilks, D. S.: Statisitcal Methods in the Atmospheric Sciences, Academic Press, 467 pp., 1995. 31652

Williams, G. P.: Circulation sensitivity to tropopause height, J. Atmos. Sci., 63, 1954–1961, 2006. 31647

Yin, J. H.: A consistent poleward shift of the strom tracks in simulations of 21st century climate, Geophys. Res. Lett., 32, L18701, doi:10.1029/2005GL023684, 2005. 31645

Zhou, Y. P., Xu, K.-M., Sud, Y. C., and Betts, A. K.: Recent trends of the tropical hydrological cycle inferred from Global Precipitation Climatology Project and International Satellite Cloud Climatology Project data, J. Geophys. Res., 116, D09101, doi:10.1029/2010JD015197, 2011. 31645

ACPD

11, 31643–31688, 2011

Table 1. Stratospheric cooling experiments.

Signal	Description
10PLO3	Global 10 % reduction in stratospheric ozone
$10PLO3_{TR}$	As 10PLO3, but ozone reduced over tropics (±30°) only
$10PLO3_{ML}$	As 10PLO3, but ozone reduced over mid-latitudes (30–60° N/S)
$10PLO3_{HL}$	As 10PLO3, but ozone reduced over high-latitudes (60–90° N/S)

ACPD
11, 31643–31688, 2011

Table 2. Tropospheric heating experiments.

Signal	Description
LTHT	Global lower-tropospheric (surface to ~700 hPa) heating of 0.1 K day^{-1}
$LTHT_{TR}$	As LTHT, but heating of tropics (±30°) only
$LTHT_{ML}$	As LTHT, but heating of mid-latitudes (30–60° N/S)
$LTHT_{HL}$	As LTHT, but heating of high-latitudes (60–90° N/S)
$LTHT_{TRML}$	As LTHT, but heating of tropics and mid-latitudes (±60°)
$LTHT_{MLHL}$	As LTHT, but heating of mid- and high-latitudes (±30–90°)
LTHT2x	As LTHT, but double the heating rate (0.2 K day^{-1})
LTHT4x	As LTHT, but quadruple the heating rate (0.4 K day^{-1})
MTHT	Heating the mid-troposphere (~700–400 hPa)
$UTHT_{ML}$	Mid-latitude heating of the upper troposphere (4 levels below tropopause)

ACPD
11, 31643–31688, 2011

Table 3. Definition of the CMIP3 2xCO2 equilibrium (slab ocean) and the 1 % to 4xCO2 transient experiments used in this study. A "Y" ("N") indicates this model was (was not) used for the given experiment.

Model Acronym	Institution	2xCO2	4xCO2
CCSM3	National Center for Atmospheric Research	Y	Y
CGCM3.1(T47)	Canadian Center for Climate Modeling and Analysis	Y	Y
CGCM3.1(T63)	Canadian Center for Climate Modeling and Analysis	Y	N
CSIRO-Mk3.0	CSIRO Atmospheric Research	Y	N
ECHAM5/MPI-OM	Max Plank Institute for Meteorology	Y	N
GFDL-CM2.0	Geophysical Fluid Dynamics Laboratory	Y	Y
GFDL-CM2.1	Geophysical Fluid Dynamics Laboratory	N	Y
GISS-ER	Goddard Institute for Space Studies	Y	Y
INM-CM3.0	Institute for Numerical Mathematics	Y	Y
IPSL-CM4	Institut Pierre Simon Laplace	N	Y
MIROC3.2(hires)	Center for Climate System Research/NIES[a]/JAMSTEC[b]	Y	N
MIROC3.2(medres)	Center for Climate System Research/NIES[a]/JAMSTEC[b]	Y	Y
MRI-CGCM2.3.2	Meteorological Research Institute	Y	Y
PCM	National Center for Atmospheric Research	N	Y
UKMO-HadGEM1	Hadley Center for Climate Prediction and Research	Y	N

[a] NIES is the National Institute for Environmental Studies.

[b] JAMSTEC is the Frontier Research Center for Global Change in Japan.

ACPD
11, 31643–31688, 2011

Table 4. Tropospheric (850–300 hPa) poleward jet displacements for the (top) stratospheric cooling experiments and (middle & bottom) tropospheric heating/global warming experiments. Units are degrees latitude. CAM experiment significance is based on a Student's *t*-test and is denoted by bold (≥90 %); * (≥95 %) and ** (≥99 %). Also included is the corresponding jet displacement based on the ensemble mean of 12 CMIP3 2xCO2 equilibrium experiments and 10 CMIP3 4xCO2 transient experiments.

Signal	ANN		DJF		MAM		JJA		SON	
	NH	SH	NH	SH	NH	SH	NH	SH	NH	SH
10PLO3	0.30	**0.59***	0.35	**0.64**	**0.67**	0.10	−0.15	0.72	0.38	**0.87***
$10PLO3_{HL}$	0.31	**0.40***	−0.07	0.47	**0.84**	0.31	0.39	0.13	0.12	**0.69***
$10PLO3_{ML}$	0.40	0.26	0.42	0.05	0.60	0.19	0.34	0.04	0.31	**0.81***
$10PLO3_{TR}$	−0.04	−0.12	−0.20	−0.50	−0.01	**−0.60**	−0.05	0.32	0.14	0.30
LTHT	0.33	−0.13	0.49	−0.17	0.70	−0.34	−0.01	−0.17	0.17	0.18
$LTHT_{HL}$	−0.26	−0.16	−0.26	0.01	−0.14	**−0.46**	−0.65	−0.18	−0.06	0.01
$LTHT_{ML}$	**0.66***	**1.02****	0.34	**0.89****	**0.79**	**0.92****	**0.74**	**1.15***	**0.78****	**1.16***
$LTHT_{TR}$	−0.05	−0.09	0.23	**−0.63**	0.28	−0.31	−0.49	0.42	−0.22	0.16
LTHT2x	0.12	**−0.73****	**0.66**	**−0.94****	**0.67**	**−0.60**	**−0.64**	−0.40	−0.21	**−0.95***
$LTHT2x_{HL}$	−0.32	**−0.42***	−0.19	**−0.77***	0.19	**−0.77***	**−0.94**	−0.11	−0.29	0.06
$LTHT2x_{ML}$	**1.67****	**0.85***	**1.90****	**0.72***	**1.70****	**1.01****	**1.56****	**0.93**	**1.56****	0.65
$LTHT2x_{TR}$	−0.20	−0.03	0.39	−0.32	0.36	**−0.57***	**−1.22****	0.54	−0.26	0.18
LTHT4x	−0.34	**−1.12****	**0.63***	**−1.37****	−0.06	**−1.03****	**−1.49****	**−1.05***	**−0.41**	**−0.97****
$UTHT_{ML}$	**0.65***	**0.53****	**0.59**	0.22	**1.10***	**0.75***	0.43	0.53	0.46	**0.69**
2xCO2	**1.08****	0.09	**1.34****	−0.10	**1.70****	0.28	0.50	0.35	**0.71****	−0.20
8xCO2	**1.50****	0.03	**1.44****	−0.21	**2.65****	**1.27****	0.55	0.04	**1.50****	**−1.05***
2xCO2 CMIP3	0.46	0.73	0.58	1.22	−0.01	1.13	0.56	0.36	0.67	0.20
4xCO2 CMIP3	0.98	1.74	0.66	1.72	0.81	2.20	1.54	1.91	0.98	1.14

ACPD
11, 31643–31688, 2011

Table 5. Annual mean poleward displacement (degrees latitude) of several measures of tropical width for the (top) stratospheric cooling experiments and (middle & bottom) tropospheric heating/global warming experiments, including the CMIP3 2xCO2 and 4xCO2 ensemble mean. These measures are based on the subtropical dry zone (precipitation minus evaporation, $P-E$), mean meridional mass circulation (MMC) and the tropospheric (850–300 hPa) jet. See text for further description. Significance is denoted as in Table 4.

Signal	P−E		MMC		Jet	
	NH	SH	NH	SH	NH	SH
10PLO3	**0.29**	**0.30****	0.11	**0.15**	0.30	**0.59***
$10PLO3_{HL}$	0.21	**0.22***	0.04	**0.17**	0.31	**0.40***
$10PLO3_{ML}$	0.23	**0.23***	0.12	0.13	0.40	0.26
$10PLO3_{TR}$	−0.13	0.03	−0.18	−0.02	−0.04	−0.12
LTHT	0.14	**0.21***	−0.02	0.02	0.33	−0.13
$LTHT_{HL}$	−0.13	0.13	−0.07	0.03	−0.26	−0.16
$LTHT_{ML}$	**0.61****	**0.67****	**0.32***	**0.29****	**0.66***	**1.02****
$LTHT_{TR}$	−0.18	0.01	−0.17	−0.11	−0.05	−0.09
LTHT2x	0.16	0.01	−0.16	−0.04	0.12	**−0.73****
$LTHT2x_{HL}$	**−0.41****	0.02	−0.17	−0.13	−0.32	**−0.42***
$LTHT2x_{ML}$	**1.03****	**0.64****	**0.79****	**0.33***	**1.67****	**0.85***
$LTHT2x_{TR}$	**−0.34***	0.01	**−0.36****	−0.07	−0.20	−0.03
MTHT2x	**0.66****	**0.41****	**0.47****	**0.18**	**0.74***	**0.48***
$MTHT2x_{HL}$	**−0.30***	**−0.22***	−0.10	−0.11	−0.29	**−0.69****
$MTHT2x_{ML}$	**1.16****	**1.03****	**0.91****	**0.40****	**1.46****	**1.29****
$MTHT2x_{TR}$	**−0.43****	0.05	−0.10	**0.23***	0.02	**0.45***
LTHT4x	−0.18	−0.05	**−0.31***	−0.14	−0.34	**−1.12****
MTHT	**0.24**	**0.20***	0.01	0.10	0.31	0.23
MTHT4x	**0.74****	**0.55****	**0.41****	**0.32****	**0.74****	**0.42***
$UTHT_{ML}$	**0.40****	**0.26***	**0.28***	**0.20***	**0.65***	**0.53****
$LTHT_{TRML}$	**0.34***	**0.29****	0.02	0.02	0.41	0.20
$LTHT2x_{TRML}$	**0.60****	**0.36****	**0.21**	**0.18***	**0.97****	**0.53****
$LTHT_{MLHL}$	**0.28***	**0.33****	0.16	0.07	0.28	0.14
$LTHT2x_{MLHL}$	**0.56****	**0.56****	**0.43****	**0.33****	**0.43**	0.39
2xCO2	**0.83****	**0.60****	**0.81****	**0.42****	**1.08****	0.09
8xCO2	**0.85****	**1.56****	**1.48****	**1.41****	**1.50****	0.03
2xCO2 CMIP3	0.31	0.90	0.52	0.86	0.46	0.73
4xCO2 CMIP3	1.23	1.33	0.73	1.34	0.98	1.74

ACPD
11, 31643–31688, 2011

Table 6. Northern Hemisphere 850–20 hPa percent change in wave refraction for the (top) stratospheric cooling experiments and (bottom) global warming experiments. Also included is the mid-latitude, lower tropospheric heating experiments ($LTHT_{ML}$ and $LTHT2x_{ML}$), as well as the ensemble mean CMIP3 2xCO2 wave refraction. Wave refraction is estimated as the meridional component of EP flux divided by the vertical component. A more positive value indicates more equatorward wave propagation.

Signal	DJF	MAM	JJA	SON
10PLO3	2	15	−26	5
$10PLO3_{HL}$	1	35	−25	−8
$10PLO3_{ML}$	21	25	−8	−2
$10PLO3_{TR}$	5	20	−29	−8
LTHT	19	21	−25	−3
LTHT2x	23	38	−22	−7
LTHT4x	26	−32	−31	−17
2xCO2	33	56	−12	4
8xCO2	49	49	38	15
$LTHT_{ML}$	3	8	−13	−8
$LTHT2x_{ML}$	39	12	−16	2
2xCO2 CMIP3	13	15	−13	24

ACPD
11, 31643–31688, 2011

Table 7. Tropospheric (850–300 hPa) warming amplification factors for high-latitudes (HL; 60–90° minus 30–60°) and mid-latitudes (ML; 30–60° minus 0–30°) for the global warming experiments. Factors are based on log-pressure and area weighting. Also included are the corresponding values based on the ensemble mean of 12 CMIP3 2xCO2 experiments. Units are K.

Signal		ANN		DJF		MAM		JJA		SON	
		HL	ML	HL	ML	HL	ML	HL	ML	HL	ML
LTHT	NH	0.02	−0.01	−0.01	−0.13	−0.14	−0.02	0.22	0.08	−0.02	0.02
	SH	0.22	0.03	0.24	−0.04	0.27	0.05	0.23	0.05	0.16	0.05
LTHT2x	NH	0.16	−0.13	−0.06	−0.29	0.01	−0.12	0.41	−0.08	0.24	−0.04
	SH	0.62	−0.02	0.62	−0.11	0.56	0.07	0.63	0.02	0.67	−0.07
LTHT4x	NH	0.64	−0.21	0.40	−0.47	0.35	−0.30	1.15	−0.03	0.66	−0.02
	SH	1.02	−0.01	0.94	−0.17	0.93	0.15	1.18	0.03	1.03	−0.03
2xCO2	NH	−0.05	0.21	−0.15	−0.03	−0.37	0.16	0.24	0.35	0.07	0.36
	SH	0.36	0.22	0.29	0.27	0.30	0.31	0.45	0.17	0.43	0.13
8xCO2	NH	1.08	1.10	1.04	−0.03	0.10	0.52	2.11	2.10	1.05	1.82
	SH	0.95	0.59	0.63	0.61	0.70	1.00	1.35	0.43	1.15	0.29
2xCO2 CMIP3	NH	0.03	−0.40	0.14	−0.40	0.10	−0.39	−0.07	−0.02	−0.05	0.02
	SH	−0.23	−0.41	−0.59	−0.21	−0.35	−0.29	0.10	−0.56	−0.08	−0.57

ACPD
11, 31643–31688, 2011

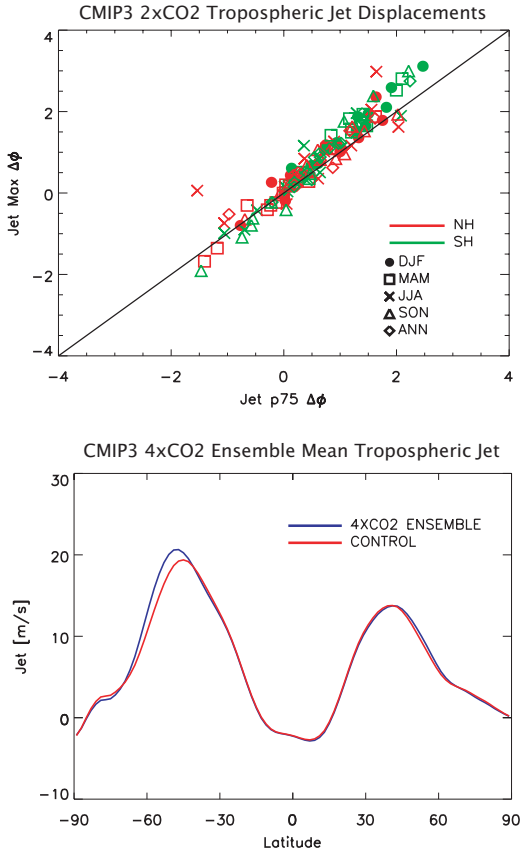

Fig. 1. (top panel) Tropospheric poleward jet displacement [degrees latitude] based on 12 CMIP3 2xCO2 equilibrium experiments using the maximum zonal wind method (Jet Max) and the percentile method with the 75th percentile (Jet p75). (bottom panel) The ensemble annual zonal mean tropospheric jet (850–300 hPa U) response based on 10 1 % to 4xCO2 transient CMIP3 experiments, along with the corresponding control.

ACPD
11, 31643–31688, 2011

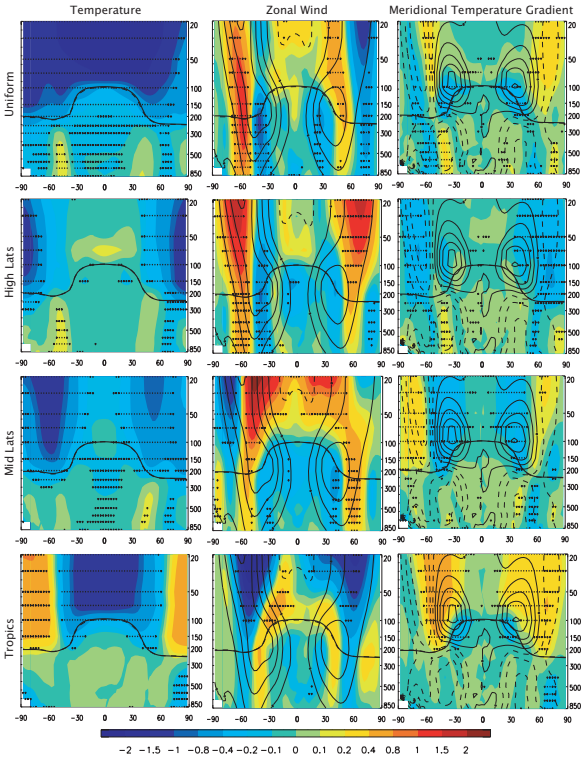

Fig. 2. Zonal annual mean (left) temperature, (center) zonal wind and (right) meridional temperature gradient response for 10PLO3 at (top) all latitudes, (middle top) high latitudes, (middle bottom) mid-latitudes and (bottom) low latitudes. Also shown is the tropopause pressure for the (dashed) control and (solid) experiment. Symbols represent significance at the 90 % (diamond); 95 % (cross) and 99 % (dot) confidence level. Climatological U (T_y) contour interval is 10 m s^{-1} (2×10^{-3} K km^{-1}) with negative values dashed. T units are K.

ACPD
11, 31643–31688, 2011

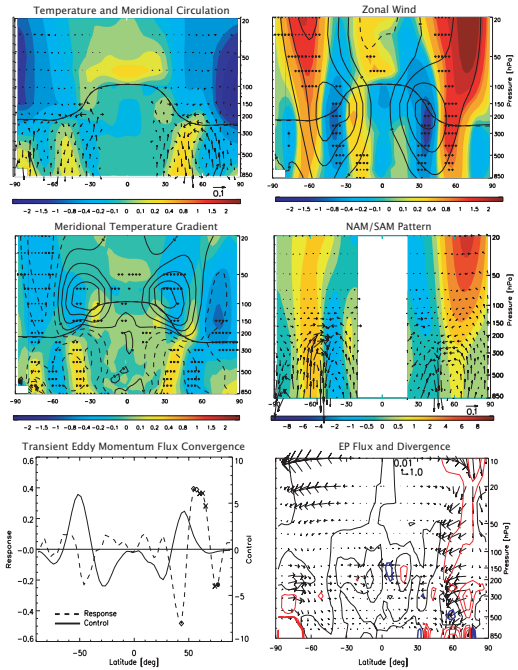

Fig. 3. MAM 10PLO3$_{HL}$ response of (top left) temperature and meridional circulation, (top right) zonal wind, (middle left) meridional temperature gradient, (middle right) SAM/NAM U pattern, (bottom left) 250 hPa transient eddy momentum flux convergence [K m s^{-1}] and (bottom right) EP flux [m^2 s^{-2}] and flux divergence [10^{-6} m s^{-2}], divided by the standard density. T_y (U) contour interval is 2×10^{-3} K km^{-1} (10 m s^{-1}) with negative values dashed. Units of NAM/SAM are m s^{-1} per standard deviation of the PC time series. Indicated vector length (top left) represents 0.1 cm s^{-1} for the meridional component and -0.1×10^{-4} Pa s^{-1} for the vertical component. EP flux divergence contour interval is [−6, −4, −2, 0, 2, 4, 6], with negative values blue and positive values red. Symbols represent significance as in Fig. 2.

ACPD
11, 31643–31688, 2011

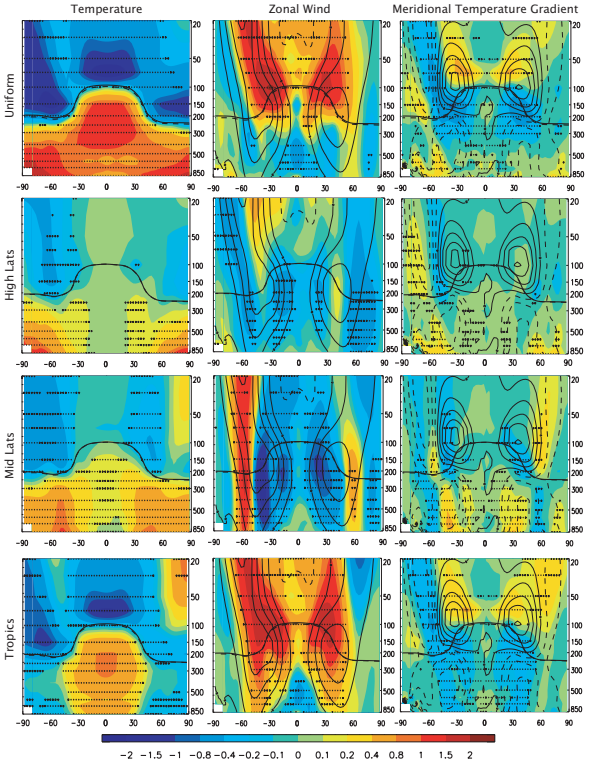

Fig. 4. As in Fig. 2, but based on the lower tropospheric heating (LTHT) experiments.

ACPD
11, 31643–31688, 2011

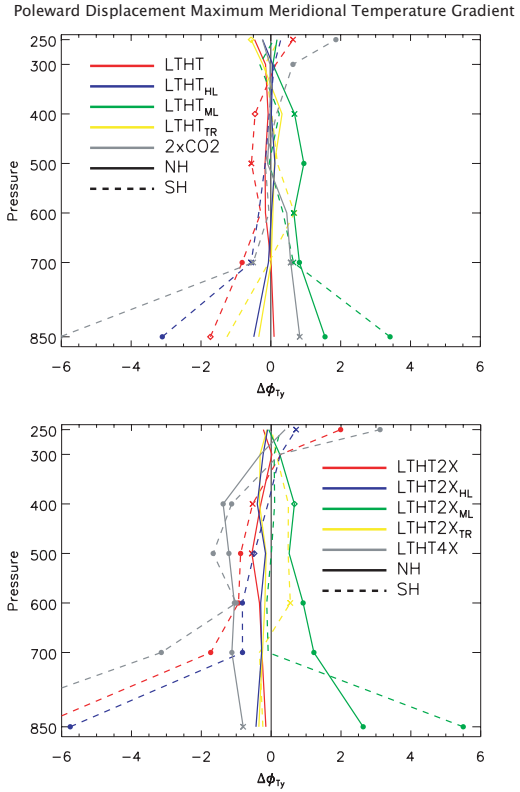

Fig. 5. Poleward displacement of the latitude of the maximum tropospheric temperature gradient (T_y) for the Northern (solid) and Southern (dashed) Hemisphere.

ACPD
11, 31643–31688, 2011

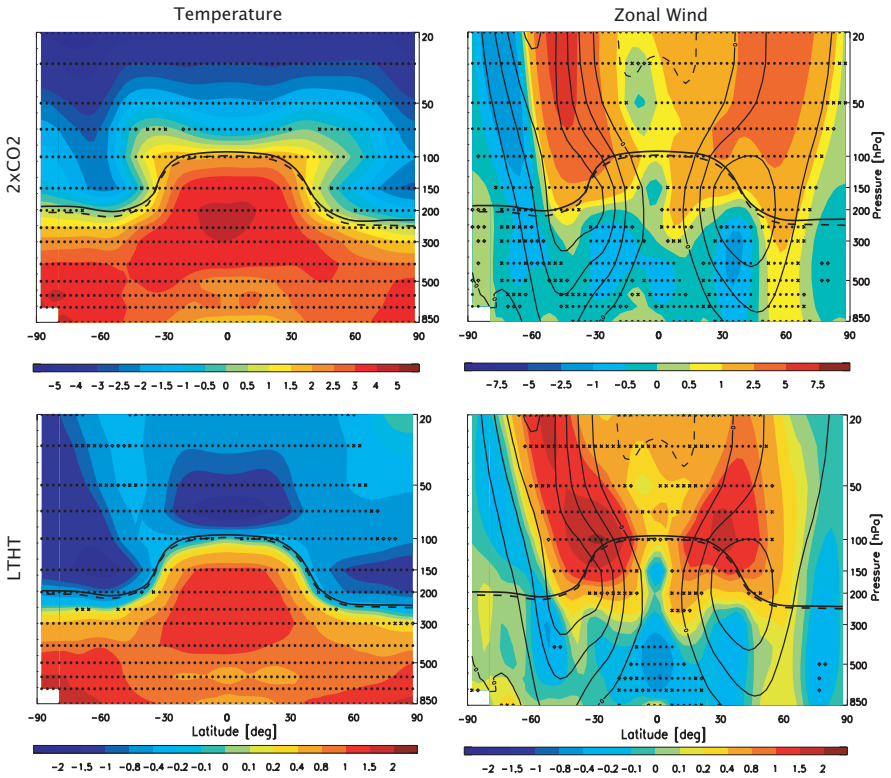

Fig. 6. 2xCO2 (top) and LTHT (bottom) annual mean temperature (left) and zonal wind (right) response. LTHT results are as in Fig. 4. Note contour differences between 2xCO2 and LTHT.

ACPD
11, 31643–31688, 2011

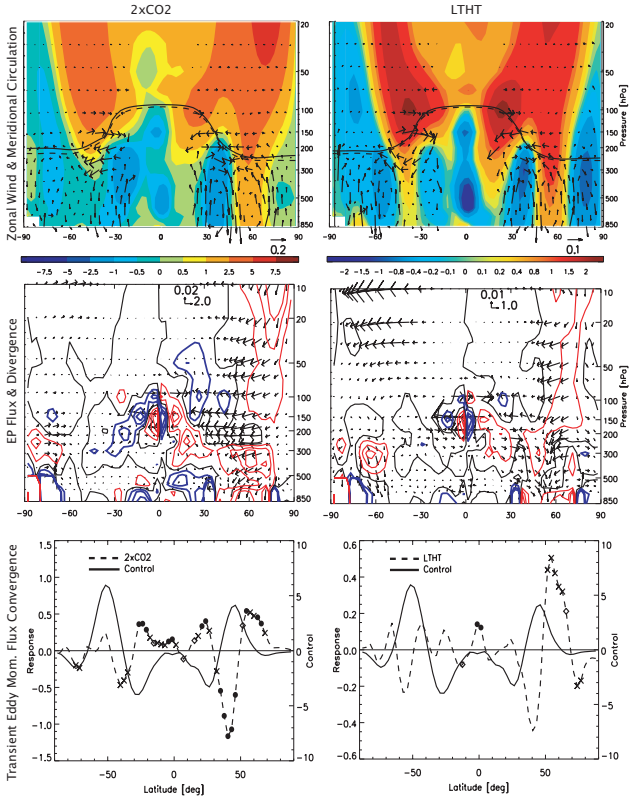

Fig. 7. 2xCO2 (left) and LTHT (right) MAM zonal wind and meridional circulation (top), EP flux and divergence (middle) and transient eddy momentum flux convergence (bottom) response. Units and EP divergence contour interval are as in Fig. 3. Note scale differences between 2xCO2 and LTHT.

ACPD
11, 31643–31688, 2011

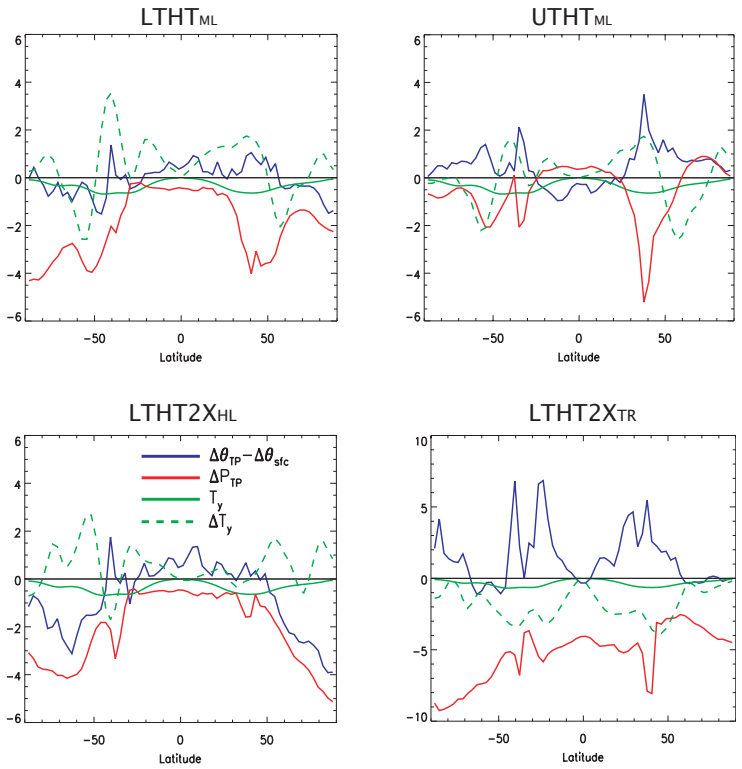

Fig. 8. Annual mean gross dry static stability change (blue; $\Delta\theta_{TP} - \Delta\theta_{sfc}$), tropopause pressure change (red; ΔP_{TP}), climatological baroclinicity at 500 hPa (green solid; T_y) and the corresponding response (green dashed; ΔT_y) for (top left) LTHT$_{ML}$, (top right) UTHT$_{ML}$, (bottom left) LTHT2x$_{HL}$ and (bottom right) LTHT2x$_{TR}$. Units are K, hPa, K km^{-1} 10^{-4} and K km^{-1} 10^{-2}, respectively.

ACPD
11, 31643–31688, 2011

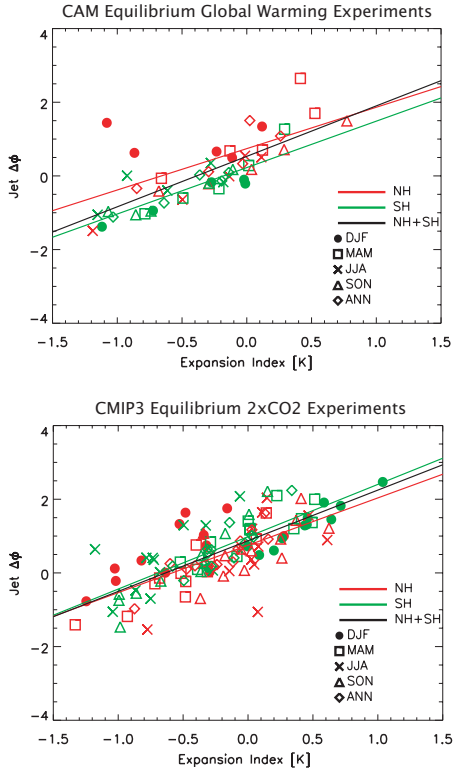

Fig. 9. Scatterplot of tropospheric poleward jet displacement versus the expansion index for the (top panel) CAM global warming equilibrium experiments (LTHT, LTHT2x, LTHT4x, 2xCO2, 8xCO2) and (bottom panel) 12 CMIP3 2xCO2 equilibrium experiments. The expansion index is defined as the difference in mid-latitude (30–60° minus 0–30°) and high-latitude (60–90° minus 30–60°) tropospheric warming amplification. Also included are the corresponding linear regression lines, all of which are significant at the 99 % confidence level.

ACPD
11, 31643–31688, 2011